Detection of a Distinctive Genomic Signature in Rhabdoid Glioblastoma, A Rare Disease Entity Identified by Whole Exome Sequencing and Whole Transcriptome Sequencing[1,2,3]

Youngil Koh[*,§,4], Inho Park[†,4], Chung-Hyun Sun[†], Seungmook Lee[†], Hongseok Yun[†], Chul-Kee Park[‡,§], Sung-Hye Park[§,¶], Joo Kyung Park[*] and Se-Hoon Lee[*,§]

[*]Department of Internal Medicine, Seoul National University Hospital, 101 Daehak-ro, Jongno-gu, Seoul 110-744, Korea; [†]Bioinformatics Group, Platform Development Center, CSP R&D, Samsung SDS, East Campus, Samsung SDS Tower, 123 Olympic Ro 35 Gil, Songpa-gu, Seoul 138-240, Korea; [‡]Department of Neurosurgery, Seoul National University Hospital, 101 Daehak-ro, Jongno-gu, Seoul 110-744, Korea; [§]Cancer Research Institute, Seoul National University College of Medicine, 101 Daehak-ro, Jongno-gu, Seoul 110-799, Korea; [¶]Department of Pathology, Seoul National University Hospital, 101 Daehak-ro, Jongno-gu, Seoul 110-744, Korea

Abstract

We analyzed the genome of a rhabdoid glioblastoma (R-GBM) tumor, a very rare variant of GBM. A surgical specimen of R-GBM from a 20-year-old woman was analyzed using whole exome sequencing (WES), whole transcriptome sequencing (WTS), single nucleotide polymorphism array, and array comparative genomic hybridization. The status of gene expression in R-GBM tissue was compared with that of normal brain tissue and conventional GBM tumor tissue. We identified 23 somatic non-synonymous small nucleotide variants with WES. We identified the *BRAF* V600E mutation and possible functional changes in the mutated genes, *ISL1* and *NDRG2*. Copy number alteration analysis revealed gains of chromosomes 3, 7, and 9. We found loss of heterozygosity and focal homozygous deletion on 9q21, which includes *CDKN2A* and *CDKN2B*. In addition, WTS revealed that *CDK6*, *MET*, *EZH2*, *EGFR*, and *NOTCH1*, which are located on chromosomes 7 and 9, were over-expressed, whereas *CDKN2A/2B* were minimally expressed. Fusion gene analysis showed 14 candidate genes that may be functionally involved in R-GBM, including *TWIST2*, and *UPK3BL*. The *BRAF* V600E mutation, *CDKN2A/2B* deletion, and *EGFR/MET* copy number gain were observed. These simultaneous alterations are very rarely found in GBM. Moreover, the *NDRG2* mutation was first identified in this study as it has never been reported in GBM. We observed a unique genomic signature in R-GBM compared to conventional GBM, which may provide insight regarding R-GBM as a distinct disease entity among the larger group of GBMs.

Translational Oncology (2015) 8, 279–287

http://dx.doi.org/10.1016/j.tranon.2015.05.003

Introduction

Rhabdoid glioblastoma (R-GBM) is a very rare disease with few cases reported [1–8]. R-GBM is characterized by tumor cells that resemble rhabdomyoblasts [2], which robustly express vimentin, epithelial membrane antigen (EMA), and SMARCB1 (INI-1), but only faintly express glial fibrillary acidic protein (GFAP) [5,7,9,10]. Clinically, R-GBMs can occur at any age but most commonly occur in teenagers younger than 20 years old [1,2,5].

Chromosome 22, which is frequently lost in atypical teratoid rhabdoid tumors (ATRT), is often deleted in these tumors [3,8], although this finding is inconsistent [1]. In one case, copy number gains were noted for chromosomes 3, 7, 9, 12, 17q, and 21q [1] in R-GBM. Also, in a case series, copy number gain or amplification of *EGFR* on chromosome 7 was noted [9]. Regarding genetic changes prevalent in brain tumors, *CDKN2A* hemizygous deletion was reported in one case [2]. Otherwise, *BRAF* mutations were absent in two cases that were examined [11], and *SMARCB1* (INI-1) [12,13], which is important in ATRT, was not mutated in R-GBM [2].

Presently, R-GBM is not recognized as a distinct disease entity by the World Health Organization [14] classification system because accumulated information on this rare variety is still rudimentary. To our knowledge, no study has evaluated the genome-wide profile of this disease except for one case that was evaluated using array comparative genomic hybridization (CGH) [1]. To determine whether R-GBM should be recognized as a disease that is distinct from conventional glioblastoma (GBM) or other tumors with similar characteristics such as ATRT, comprehensive genomic data will be fundamental for diagnostic, prognostic, and therapeutic decisions.

A 20-year-old female presented with a rim-enhanced tumor that was pathologically proven to be an R-GBM. She underwent two extensive surgeries and concurrent chemoradiotherapy combined with oral temozolomide treatment. She was free of disease for 25 months after the treatment. Using next generation sequencing techniques, we studied this tumor to obtain novel insight into identifying distinctive genetic changes in an R-GBM compared to conventional GBM as well as normal brain tissue. We performed whole exome sequencing (WES), whole transcriptome sequencing (WTS), single nucleotide polymorphism (SNP) array, and array-CGH. The aims of this study were to investigate the genomic profile of R-GBM and to explore whether R-GBM had a distinct genomic signature that could be used as a therapeutic target.

Materials and Methods

Study Patient

A 20-year-old female patient was seen in an outpatient clinic at Seoul National University Hospital because of headache, nausea, and vomiting in April 2011. Brain magnetic resonance imaging showed a 5-cm sized, well-enhanced mass in the right temporal lobe. The mass also showed diffusion restriction with increased perfusion at the peripheral enhanced portion. She underwent a craniotomy for tumor removal in May 2011. The molecular genetic characteristics of the surgical specimen were evaluated as follows. Immunohistochemical staining revealed focal expression of GFAP and strong expression of EMA and INI-1 (Figure 1). Fluorescence *in situ* hybridization (FISH) showed no *EGFR* amplification and no deletion of chromosomes 1p, 9p21, or 19q. In addition, methylation-specific PCR showed hypermethylation of the *MGMT* promoter, and the MIB-1 labeling index was measured as 36.5% with an Aperio Spectrum plus image analyzer. The study patient received adjuvant concurrent
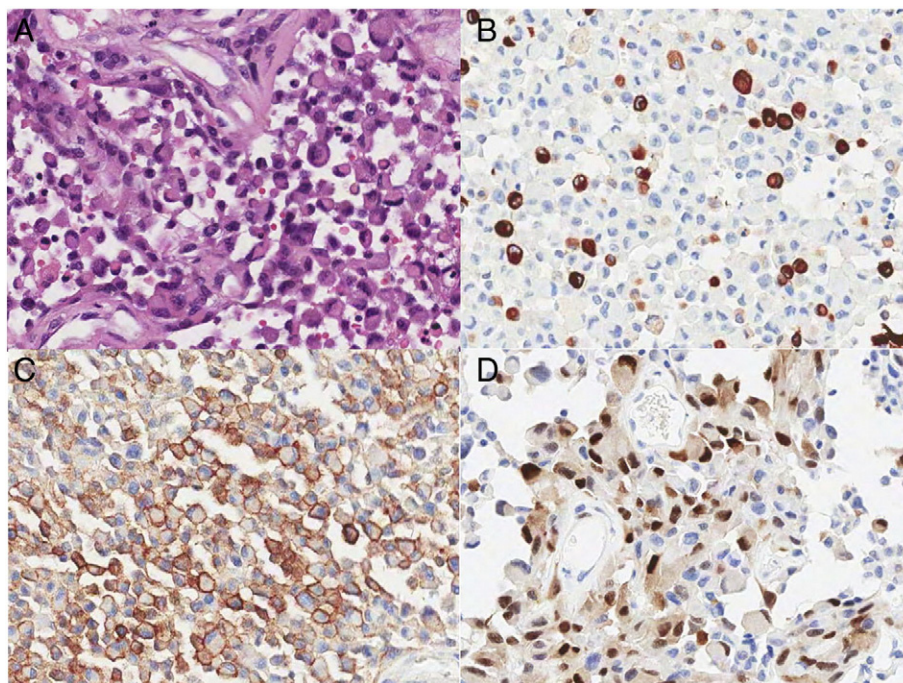
Figure 1. Pathology of rhabdoid glioblastoma. (A) A representative H&E picture shows non-cohesive rhabdoid cells with eccentrically located pleomorphic nuclei and eosinophilic globular cytoplasm (H&E, original magnification ×200). (B) GFAP is robustly positive in some, but not all, tumor cells (GFAP immunostaining, original magnification ×200). (C) EMA is strongly positive in a cytoplasmic membrane pattern in almost all tumor cells (EMA immunohistochemistry, original magnification ×200). (D) Cyclin D1 (CCND1) staining is strongly positive in the nuclei of the tumor cells (cyclin D1 immunohistochemistry, original magnification ×200).

chemoradiotherapy with oral temozolomide treatment after the surgery. However, the tumor recurred on the ipsilateral side of the frontal lobe, and she underwent a second operation to remove the recurrent tumor. The final pathology confirmed that, as with the initial mass, the recurrent tumor was an R-GBM. The recurrent tumor had a MIB-1 labeling index of 37.5%. She has been free from disease for 25 months as of December 2013. The study protocol was reviewed and approved by the institutional review board of the Seoul National University Hospital, and informed consent was obtained from the study patient. The recommendations of the Declaration of Helsinki for biomedical research involving human subjects were followed.

DNA and RNA Preparation

Fresh frozen tumor tissue and 5 ml peripheral blood were obtained at the time of the first surgery. The DNeasy® Blood & Tissue Kit (Qiagen, Hilden, Germany) was used to extract genomic DNA and tumor DNA, according to the manufacturer's recommendations. Extracted DNA was quantified using a NanoDrop ND-1000 spectrophotometer (NanoDrop Technologies, Wilmington, DE). RNA was extracted from the tumor tissue using TRIzol (Invitrogen, Grand Island, NY) and eluted in RNAse-free water. RNA quantity and quality were assessed using an Agilent 2100 Bioanalyzer (Agilent Technologies Inc., Santa Clara, CA).

Whole Exome Sequencing

We used the Agilent SureSelect50-Mb ExomeCapture Kit for exon target enrichment (Agilent Technologies Inc.). Sequencing was performed using the Illumina HiSeq2000 (Illumina Inc., San Diego, CA) with 100-bp paired-end reads. Using UCSC hg19 as a reference genome, mapping and pairing were performed with the Burrows-Wheeler Aligner (BWA) algorithm [15]. Local realignment was performed using Genome Analysis ToolKit (GATK) [16], and duplication removal was conducted using Picard.

Somatic calling of somatic single nucleotide variants (SNVs) and indels is described in Supplement 1. Using SnpEff [17], we selected variations that were non-synonymous and rare in the general population (defined as <1% in the 1000 genome project (http://www.1000genomes.org/)). For copy number alteration (CNA) analysis of WES data, we used the Copy Number Analysis for Targeted Resequencing (CONTRA) tool [18] and summarized the exon-level log2 fold changes of read depth between the normal and tumor samples into gene-level log2 fold changes. Loss of heterozygosity (LOH: heterozygous in normal tissue but homozygous in the tumor) analysis also was performed using WES. We used variant allele fraction values of normal and tumor samples to determine the LOH region.

Whole Transcriptome Sequencing

The 200- to 500-bp double-stranded cDNA fragments were purified by agarose gel electrophoresis and amplified using PCR to produce the library. Raw sequencing reads were produced by Illumina HiSeq 2000 with 100-bp paired-end reads. After removing noisy raw reads, which contained the adaptor sequence and more than 10% unknown bases or low quality bases, the remaining reads were aligned with the human reference genome (UCSC hg19). To find fusion transcripts, we utilized three types of fusion discovery software: deFuse [19], BreakFusion [20], and ChimeraScan [21]. UniGene clusters were downloaded from the National Center for Biotechnology Information (http://www.ncbi.nlm.nih.gov/) to assist in locating potential gene fusions. To quantify the gene expression level, the number of reads that mapped to the exons of each RefSeq gene was calculated, and the corresponding reads per kilobase per million reads (RPKM) [22] value was derived. Possible functional fusions were annotated using Oncofuse [23] and went through further analysis.

SNP Array

We applied a genome-wide SNP array (Illumina HumanOmni5-Quad BeadChip, Illumina) using the genomic DNA sample. With B allele frequency data from GenomeStudio (Illumina) analysis results for SNP array data, we used the paired parent-specific circular binary segmentation method for LOH and CNA analysis.

Array Comparative Genomic Hybridization and Identification of CNAs

We used the Agilent aCGH G3 Human 1×1M array with tumor and matched normal genomic DNA samples. Raw data were acquired and normalized using the locally weighted scatterplot smoothing (LOWESS) algorithm using Feature Extraction software ver10.7 (Agilent software). The significance test for each CNV region used the Z-statistic calculated by DNA Analytics ver4.0.81 (Agilent software), which sets the window size to 1M and Z-score threshold to 4.0.

Use of the Public Database as a Reference

We used gene expression data estimated from WTS to select possible functional genetic changes in our study. Because R-GBM is a rare disease and obtaining control samples is not easy, we used a public database as a reference. First, we compared the RPKM value of specific genetic changes found in our analysis with normal brain expression values. Then, we compared the RPKM value of specific genetic changes found in our analysis with GBM data to determine whether R-GBM is simply a subtype of GBM. For the normal brain data, we used the normalized expression dataset from BrainSpan (http://www.brainspan.org/). For the GBM data, we used datasets from TCGA (https://tcga-data.nci.nih.gov) and cBioPortal for Cancer Genomics (http://www.cbioportal.org).

Results

Tumor Purity, Alignment, and Coverage Statistics

The purity of the tumor samples was estimated using SNP array data with the Allele-specific copy number analysis of tumors (ASCAT) algorithm [24]. The proportion and the ploidy of tumor cells in the sample were about 89% and 2.17, respectively (Online Resource Section 1: Supplementary Figure 1). In WES, the total numbers of uniquely mapped reads were 181,350,341 and 186,695,100 for normal and tumor samples, respectively. These data yielded mean target coverages of 210 and 197 for the samples, respectively (Online Resource Section 2: Supplementary Table 1).

Somatic SNVs and Small Indels Found With WES

We found 46,468 (45,045 in dbSNP138) and 46,191 (44,748 in dbSNP138) SNVs from the paired normal DNA and tumor DNA, respectively. A total of 45,542 (44,264 in dbSNP138) SNVs were commonly observed in both samples. We identified 3753 (3362 in dbSNP137) and 3678 (3314) small indels from the paired normal and tumor DNA, respectively. A total of 3594 (3273 in dbSNP138) small indels were common in both samples (Online Resource Section 3 and 4: Supplementary Figures 2–4). The somatic calling method is described in the Supplement Text (Online Resource Section 4). As a result, 38 somatically mutated SNVs and one small indel were

detected with WES. Twenty-three non-synonymous SNVs (Table 1) were found, 13 of which were also found with WTS.

Loss of Function SNVs and Analysis of Small Indels (Online Resource Section 5)

The candidates for loss of function were selected from the nonsense, splice junction, and frameshift variants (Supplementary Table 3 of Online Resource Section 5).

Whole Chromosome Copy Gains and Losses

Gains were identified in chromosomes 3, 7, and 9 from the SNP array and WES data (Figure 2). Interestingly, chromosome 9 showed a homozygous deletion of the 9p21 locus that contains the tumor suppressor genes CDKN2A and CDKN2B (Figure 2B).

CNA Analysis Using WES and Array-CGH

CNA data were generated from array-CGH and WES. First, CNAs were analyzed with array-CGH with probe-based CNA and interval-based CNA. The probe-based method revealed that more than 80,000 CNA regions were present in tumor tissue compared to paired normal tissue. The interval-based method revealed 370 tumor-specific CNA regions. WES analysis identified 323 regions with CNAs, which included 11 genes that are well-known tumor suppressors and oncogenes [25,26]: VHL, CTNNB1, PIK3CA, EGFR, CDK6, MET, EZH2, MLL3, CDKN2A, CDKN2B, and NOTCH1 (Table 2). In addition, WES, SNP array, and array-CGH analyses showed that CDKN2A/2B were homozygously deleted. Copy number gain was observed for CTNNB1, CDK6, VHL, MLL3, EZH2, PIK3CA, EGFR, NOTCH1, and MET with WES and SNP array analyses.

Fusions Found With WTS

A total of 376 fusions were observed with WTS with deFuse [19], BreakFusion [20], and ChimeraScan [21]. Interchromosomal fusions and intrachromosomal fusions >50 kb were selected, and thus, 24 fusions (Online Resource Section 6: Supplementary Table 4) were analyzed further. Among these 24 fusions, in-frame fusions were selected for candidate genetic hallmarks in R-GBM.

Selection of Genetic Hallmarks in R-GBM

We used WTS data to investigate functional genetic changes in R-GBM, and the public database was used as a reference. First, we compared the RPKM values of specific genetic changes found between tumor and normal brain tissue (Figure 3). We focused on affected genes with more than a 4-fold change in expression and integrated the results among WES, WTS, and array-CGH. Several genes had significant SNVs, CNAs, or fusions. Among genes with SNVs, NDRG2, NKAIN2, CER1, and ISL1 were downregulated, whereas PARP9 was upregulated in the tumor sample of the study patient compared to normal brain tissue. Among genes with CNAs, NOTCH1, EGFR, CDK6, EZH2, and MET were upregulated, whereas CDKN2A and 2B were downregulated in the tumor sample of the study patient compared to normal brain tissue. These results are summarized in Table 3.

The aforementioned analysis was assumed to have identified functional genetic changes in the selected genes. In addition, RPKM values of these selected genes in GBM and R-GBM were compared (genetic changes in GBM were obtained from the TCGA database). We listed genes with more than a 2-fold difference in genetic expression between conventional GBM and R-GBM. The following significant alterations between study samples (R-GBM) and conventional GBMs were found: 1) CER1 and ISL1 had SNVs that were significantly downregulated. 2) CDKN2A and 2B were genes with CNAs and were significantly downregulated. 3) NOTCH1, EGFR, CDK6, PIK3CA, and MET were genes with CNAs and were significantly upregulated. 4) PDK1, RASSF8, FKBP15, GALNT6, ITGA6, SLC6A6, TWIST2, and UPK3BL were significantly up-regulated fusion genes correlated to R-GBM.

Search for GBMs With Similar Genetic Hallmarks in the TCGA Database

In our case, genetic hallmarks excluding fusions are summarized below (Table 3): 1) BRAF V600E; 2) NDRG2 I92F and ISL1 C234W mutation; 3) CDKN2A/2B homozygous loss; and 4) EGFR, CDK6, EZH2, NOTCH1, and MET copy number gain. Subsequently, we searched the cBioportal (TCGA provisional data) for

Table 1. List of 23 Candidate Non-Synonymous Somatic SNVs

Chr	Position	dbSNP	Ref	Alt	Transcript	Gene	Effect	AA Change	Depth$_N$	Depth$_T$	VAF$_N$	VAF$_T$	RNA-Seq (confirmed)
Chr1	27876290	.	G	C	NM_001029882.2	AHDC1	MISSENSE	H779Q	81	66	0	0.409	O
Chr1	104093621	.	C	G	NM_017619.3	RNPC3	MISSENSE	P474A	169	192	0	0.432	O
Chr2	30748467	.	G	A	NM_182551.3	LCLAT1	NONSENSE	W42*	266	259	0	0.409	X
Chr2	209201623	.	G	A	NM_015040.3	PIKFYVE	MISSENSE	G1528R	182	174	0	0.379	O
Chr3	52413954	.	G	A	NM_015512.4	DNAH1	MISSENSE	E2471K	15	34	0	0.294	O
Chr3	122247474	.	T	C	NM_031458.2	PARP9	MISSENSE	T768A	234	300	0	0.563	O
Chr5	50685703	.	C	G	NM_002202.2	ISL1	MISSENSE	C234W	78	77	0	0.455	X
Chr6	124604235	.	G	A	NM_001040214.1	NKAIN2	MISSENSE	V47I	278	264	0	0.371	X
Chr7	42962956	.	C	T	NM_002787.4	PSMA2	MISSENSE	G142R	169	176	0	0.477	O
Chr7	99170311	.	A	T	NM_001083956.1	ZNF655	MISSENSE	M229L	183	204	0	0.309	O
Chr7	140453136	rs113488022	A	T	NM_004333.4	BRAF	MISSENSE	V600E	208	294	0	0.551	O
Chr9	14720261	.	G	A	NM_005454.2	CER1	MISSENSE	P211S	163	183	0.006	0.874	X
Chr10	100189389	.	C	G	NM_000195.3	HPS1	MISSENSE	S293T	64	63	0	0.397	O
Chr11	799344	.	G	A	NM_145886.3	PIDD	MISSENSE	S899F	53	67	0	0.373	O
Chr11	124766873	.	G	A	NM_019055.5	ROBO4	MISSENSE	R119W	25	23	0	0.478	X
Chr12	49237760	.	C	G	NM_004818.2	DDX23	MISSENSE	D95H	345	269	0	0.353	O
Chr14	21490291	.	T	A	NM_201537.1	NDRG2	MISSENSE	I92F	148	148	0	0.338	X
Chr18	54424349	.	G	A	NM_015285.2	WDR7	MISSENSE	G842D	317	318	0.003	0.374	O
Chr19	6772990	.	C	T	NM_005428.3	VAV1	MISSENSE	R58C	154	139	0	0.36	X
Chr19	13211542	rs149285767	C	T	NM_005583.4	LYL1	MISSENSE	G119E	283	238	0	0.176	O
Chr22	40417337	.	C	A	NM_138435.2	FAM83F	MISSENSE	L275I	283	257	0	0.416	X
ChrX	49840621	.	T	A	NM_001127899.2	CLCN5	MISSENSE	I196N	165	141	0	0.142	X
ChrX	111698369	.	A	G	NM_001004308.2	ZCCHC16	MISSENSE	K138R	298	290	0	0.41	X

Chr, Chromosome; Ref, Reference; Alt, Alternative; AA, amino acid; VAF, Variant allele frequency.
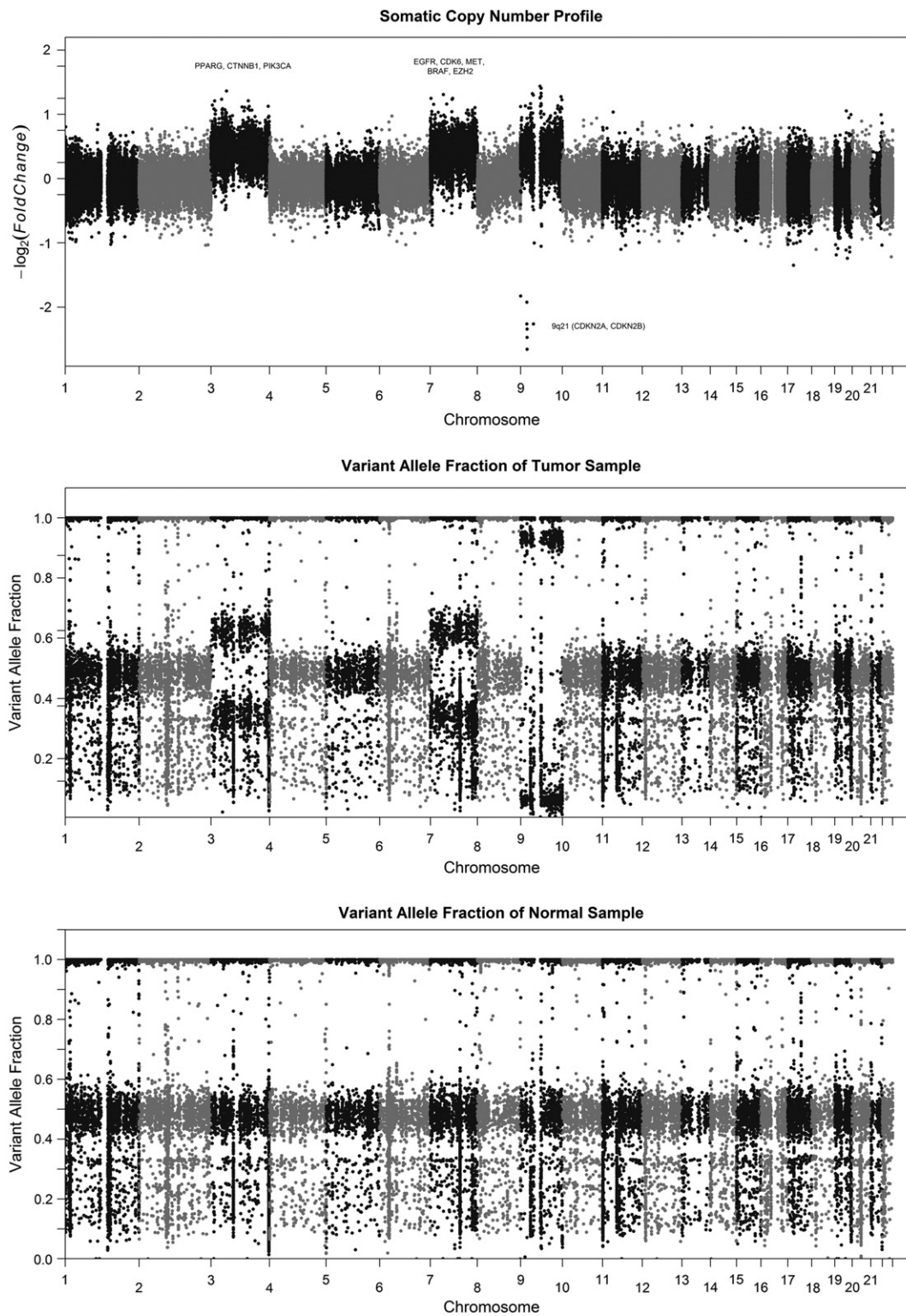
Figure 2. Copy number status of R-GBM. (A) Gross copy number changes, (B) variant allele frequency in the tumor sample, and (C) variant allele frequency in the normal sample.

GBM cases that also harbor the above mutations. For mutations, we used WES data (284 samples), and for gene copy number gain/loss, we used array-CGH data (497 samples).

Among 284 GBM cases with sequencing data, the *BRAF* V600E mutation was found in 1.7% of GBM cases. The *NDRG2* mutation was not found in GBM. However, when we searched for *NDRG2* genetic

changes in the array-CGH database, *NDRG2* was amplified in two cases (2/497 = 0.4%) and homozygously deleted in three cases (3/497 = 0.6%). For *ISL1*, no mutation was found in GBM cases. However, the *ISL1* deletion was observed in two GBM cases (2/497 = 0.4%).

Based on array-CGH data from 497 GBM cases, homozygous deletions of *CDKN2A* and *CDKN2B* were found in 62% and 61% of

Table 2. Genes with Copy Number Alterations that Are Well Known to be Associated with Cancer Development and/or Progression

Chr	Start	End	Gene	Genetic alteration	aCGH	WES	SNP array	Classification	Expression Ratio1 *	Expression Ratio2 #
Chr3	9022276	9291369	VHL	Gain	Yes	Yes	Yes	TSG	−0.28	3.07
Chr3	41240942	41281939	CTNNB1	Gain	Yes	Yes	Yes	Oncogene	−0.04	5.83
Chr3	178916609	178922393	PIK3CA	Gain	Yes	Yes	Yes	Oncogene	1.93	2.92
Chr7	55086951	55214485	EGFR	Gain	Yes	Yes	Yes	Oncogene	3.02	1.54
Chr7	92234235	92465941	CDK6	Gain	Yes	Yes	Yes	Oncogene	3.05	1.86
Chr7	116312459	116438440	MET	Gain	Yes	Yes	Yes	Oncogene	4.32	3.83
Chr7	148504464	148581441	EZH2	Gain	Yes	Yes	Yes	Oncogene	5.29	0.12
Chr7	151832010	152133090	MLL3	Gain	Yes	Yes	Yes	Oncogene	0.84	1.94
Chr9	21967751	21994490	CDKN2A	Loss	Yes	Yes	Yes	TSG	−2.38	−1.03
Chr9	22005935	22009013	CDKN2B	Loss	Yes	Yes	Yes	TSG	−3.02	−8.89
Chr9	139388896	139440238	NOTCH1	Gain	Yes	Yes	Yes	Oncogene	2.37	2.77

Chr, chromosome; aCGH, array comparative genomic hybridization; WES, whole exome sequencing; Del, deletion; TSG, tumor suppressor gene.
  * Expression ratio 1 is the log2 ratio of the expression level (value in RPKM) in our patient over the mean expression level (value in RPKM) in normal brain (http://www.brainspan.org).

  # Expression ratio 2 is the log2 ratio of the expression level (value in RPKM) in our patient over the mean expression level (value in RPKM) in glioblastoma multiforme (https://tcga-data.nci.nih.gov/tcga/tcgaHome2.jsp).

the cases, respectively. Copy number gains of *EGFR*, *CDK6*, *EZH2*, *NOTCH1*, and *MET* were found in 49%, 7%, 4.4%, 0.6%, and 8.9% of the cases, respectively. Interestingly, *NOTCH1* copy number gain, and that of *EGFR*, *CDK6*, *EZH2*, and *MET*, were mutually exclusive. Two out of three *NOTCH1*-amplified cases accompanied the *CDKN2A/B* homozygous deletion. On the other hand, copy number gains in *EGFR*, *CDK6*, *EZH2*, and *MET* were not mutually exclusive, and co-amplification of these genes was frequently seen.

In three GBM cases with the *NDRG2* homozygous deletion, two had simultaneous homozygous *CDKN2A* and *CDKN2B* deletions.
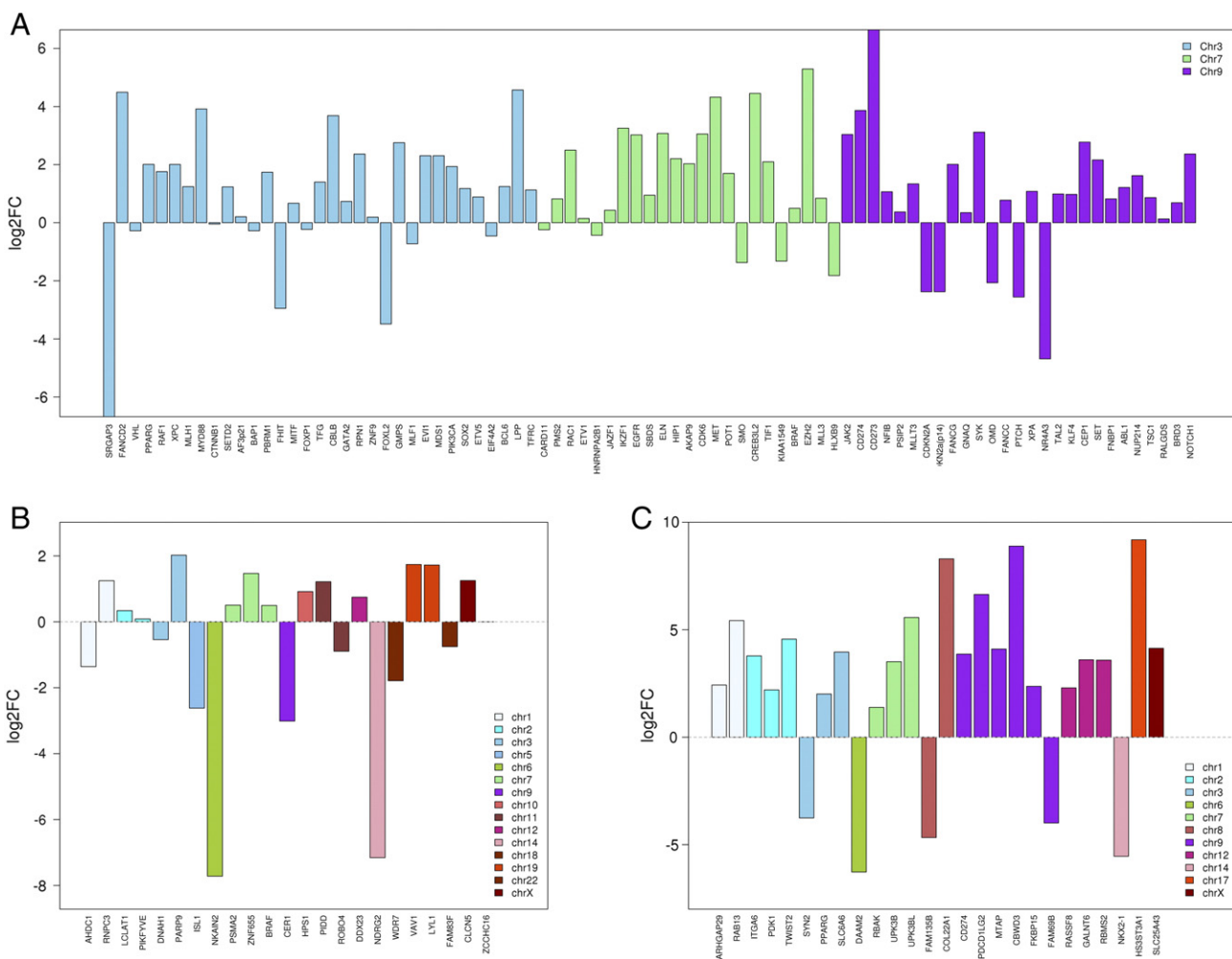

Figure 3. Expression status of selected genetic changes found in the R-GBM sample in comparison with normal brain. (A) genetic changes with copy number alteration, (B) genetic changes with single nucleotide variation, and (C) genetic changes with gene fusion (y axis shows the log2 ratio of the expression level (value in RPKM) in our patient over the mean expression level (value in RPKM) in normal brain (http://www.brainspan.org)).

Table 3. Genetic Hallmarks of Rhabdoid Glioblastoma.

Chr	Position	Change	Gene	Amino Acid Change	Ratio1 *	Ratio2 #	Frequency in GBM	Other Changes Involving This Gene in GBM
Chr5	50678958	SNV	ISL1	C234W	−2.62	−6.78	0%	Deletion (0.4%)
Chr7	140453136	SNV	BRAF	V600E	0.50	1.85	1.7%	Amplification (4.4%), deletion (0.2%)
Chr14	21490291	SNV	NDRG2	I92F	−7.16	4.80	0%	Amplification (0.4%), deletion (0.6%)
Chr3	178916609	CN gain	CDK6	NA	3.05	1.86	7%	Mutation (26%)
Chr7	55086725	CN gain	EGFR	NA	3.02	1.54	49%	None
Chr7	116335706	CN gain	MET	NA	4.32	3.83	8.9%	Mutation (0.7%)
Chr7	148504464	CN gain	EZH2	NA	5.29	0.12	4.4%	Mutation (1.1%)
Chr9	139388896	CN gain	NOTCH1	NA	2.37	2.77	0.6%	None
Chr9	21968144	CN loss	CDKN2A	NA	−2.38	−1.03	62%	Mutation (0.7%)
Chr9	22005935	CN loss	CDKN2B	NA	−3.02	−8.89	61%	Mutation (0.4%)

Chr, chromosome; CN, copy number; GBM, glioblastoma multiforme; SNV, single nucleotide variant; NA, not applicable.
* Ratio 1 is the log2 ratio of the expression level (value in RPKM) in our patient over the mean expression level (value in RPKM) in normal brain (http://www.brainspan.org).
# Ratio 2 is the log2 ratio of the expression level (value in RPKM) in our patient over the mean expression level (value in RPKM) in glioblastoma multiforme (https://tcga-data.nci.nih.gov/tcga/tcgaHome2.jsp).

In addition, two of the three GBM cases with deleted NDRG2 had a NKX2-1 homozygous deletion. Regarding gene amplification, one of the three patients had MET and EZH2 amplifications, and the other patient harbored EGFR amplification.

Among 198 GBM samples with both array-CGH and WES data, only one sample harbored the BRAF mutation, MET, EGFR, and CDK6 amplifications, and CDKN2A/B homozygous deletion at the same time. However, no patient harbored the BRAF mutation and NOTCH1 amplification at the same time. The BRAF mutation and EZH2 amplification were also mutually exclusive. To summarize, although our case of R-GBM is not representative of all R-GBMs, coexistence of the genetic hallmarks found in our patient is a very rare event in GBM.

Discussion

In this study, we addressed the genomic profile of R-GBM, a very rare disease entity. At the chromosomal level, we found copy number gains in chromosomes 3, 7, and 9, and the deletion of 9p21. When we correlate this karyotypic abnormality with genetic changes, we made the following observations.

On chromosome 3, PIK3CA was amplified, and its corresponding expression was elevated compared to normal brain. PIK3CA is frequently altered in GBM, and indeed, amplification of this gene is found in 13% of primary GBMs [27]. Hence, the PIK3CA copy number gain found in our sample was not surprising and implies that a common genetic denominator exists between GBM and R-GBM.

On chromosome 7, EGFR, EZH2, CDK6, and MET had copy number gain, and their expression was elevated compared to that in normal brain tissue. In fact, the gain of chromosome 7 along with EGFR and MET gene amplification is relatively common in adult brain tumors including GBM [28]. In addition, EGFR copy number gain and amplification were observed in a series of R-GBM cases [9,29]. On the other hand, amplification of EZH2 and CDK6 is not commonly observed; only 4% and 7% of GBM cases had amplification of these genes, respectively. Moreover, 1.2% of GBM cases had co-amplification of EZH2 and CDK6, and 0.4% (2 out of 497) of GBM cases also had co-amplification of MET, EZH2, and CDK6 according to the TCGA database. We reviewed the pathology slides of these two cases, which are detailed on the websites (cBioportal case_id=TCGA-06-0187 and cBioportal case ID= TCGA-19-1390). A pathology review of these two cases did not provide a definite diagnostic clue regarding R-GBM. Therefore, we could not draw a definite conclusion regarding whether amplification of one or more of EZH2, CDK6, or MET may be an irrelevant event or an oncogenic driver in the pathogenesis of R-GBM.

On chromosome 9, NOTCH1 copy number gain and associated over-expression were observed. Although the role of the Notch pathway in brain tumors is an area of active investigation, Notch1 signaling is known to promote survival of GBM cells via EGFR-mediated signaling [30]. In addition, Notch signaling has oncogenic potential in a model of medulloblastoma [31]. Hence, we believe that the NOTCH1 copy number gain found in our case may have substantially contributed to oncogenesis and tumor progression. However, only three among 497 cases had NOTCH1 amplification in the TCGA database, which implies that this alteration in NOTCH1 is not a common event in GBM. Regarding the genomic profile of these three cases, two harbored the CDKN2A/2B homozygous deletion as in our case, and one case harbored TP53 and IDH1 missense mutations. As mentioned in the Results section, NOTCH1 amplification was mutually exclusive with EGFR, MET, EZH2, and CDK6 amplification in the TCGA database. Hence, the simultaneous copy number gain in, and over-expression of, NOTCH1, EGFR, MET, EZH2, and CDK6 in our sample is a very interesting phenomenon. What is most interesting regarding NOTCH1 amplification is that one case with NOTCH1 amplification in the TCGA database (cBioportal case id=TCGA-02-2483) had rhabdoid features upon pathology review. Therefore, we believe that further testing for NOTCH1 copy number gain in other R-GBM samples is necessary to confirm whether NOTCH1 is a key factor for rhabdoid morphogenesis.

For chromosome 9, the 9p21 deletion (rather than chromosome 9 copy number gain) was found using WES and SNP microarray. This alteration was not detected with conventional FISH, which confirms the high sensitivity of WES and SNP microarray compared to conventional FISH. Chromosome 9p21 contains CDKN2A and CDKN2B, which are well-known tumor suppressor genes that play an important role in GBM. CDKN2A and CDKN2B were homozygously deleted in this patient, and their expression was correspondingly low. Thus, CDKN2A and CDKN2B may play an important role in our patient.

As for non-synonymous SNVs excluding BRAF V600E, we designated the ISL1 and NDRG2 mutations as genetic hallmarks of R-GBM. We selected these genes for the following reasons. First, gene expression of ISL1 and NDRG2 was significantly reduced compared to expression in normal brain, which implies that these genetic changes are functional. Second, both ISL1 and NDRG2 are biologically relevant to brain tumor development. ISL1 is required for neural development, and expression of this gene is associated with neuroendocrine carcinoma [32,33]. NDRG2 is a well-known tumor suppressor in brain tumors [34]. In contrast to our sample, ISL1 and

NDRG2 mutations were not found in the GBM TCGA database. Instead, homozygous deletion of *ISL1* (n = 2) and *NDRG2* (n = 3) was identified in a small subset (0.4% and 0.6%, respectively) of GBM cases in the TCGA database. As for the *NDRG2* deleted cases (n = 3) in the GBM (TCGA database), *KIT*, *PDGFRA*, and *CHIC2* amplifications were found in two cases (67%). Amplification of other oncogenes including *MET*, *EZH2*, *CDK4, and EGFR* was also identified. Interestingly, for tumor suppressor genes, *CDKN2A/2B* homozygous deletion (n = 2) and *NKX2-1* homozygous deletion (n = 2) were found in *NDRG2*-deleted GBMs. *NKX2-1* was also downregulated in our sample and was fused with *ARL6IP4* (Supplementary Table 4). Hence, these phenomena observed in the TCGA database coincide with the genetic changes found in our sample. More importantly, one case with the *NDRG2* deletion in the TCGA database (cBioportal case_id=TCGA-02-0281) showed possible GBM with rhabdoid features when we reviewed the histological images. Hence, we believe that loss of NDRG2 function may play an important role in R-GBM pathogenesis.

Finally, comparison of genetic changes in our case with those of ATRT is valuable because ATRT and R-GBM share common morphologic features. First, genes in the SWItch/Sucrose NonFermentable (SWI/SNF) complex, which is a genetic hallmark of ATRT [12,35,36], were not altered in R-GBM as had previously been shown. This finding suggests that although ATRT and R-GBM share common morphologic features, the SWI/SNF complex abnormality is not a key factor for rhabdoid morphogenesis. However, *EZH2* over-expression, which was recently shown to be important in ATRT [37], was observed in our sample. *EZH2* was both amplified and over-expressed in our sample. Therefore, *EZH2* copy number gain and over-expression may play an important role in rhabdoid tumor generation.

Here, we addressed genetic hallmarks found in our R-GBM case including *BRAF* V600E, *ISL1* C234W, *NDRG2* I92F, *CDKN2A/2B* deletion, *NOTCH1* copy number gain, and gain of chromosome 7 (including *CDK6*, *MET*, *EZH2*, and *EGFR* copy number gain). The patterns of mutation and gene expression in R-GBM are rather unique compared to conventional GBM, suggesting that R-GBM is a distinct disease entity. Among these genetic changes, *NOTCH1* copy number gain and *NDRG2* mutation, which are rare events in the TCGA GBM database, appear to be important genetic markers in R-GBM formation. Furthermore, *EZH2* copy number gain and over-expression may play an important role in rhabdoid tumorigenesis.

Appendix A. Supplementary data

Supplementary data to this article can be found online at http://dx. doi.org/10.1016/j.tranon.2015.05.003.

References

[1] Mutou J, Hirose Y, Ikeda E, Yoshida K, Nakazato Y, and Kawase T (2011). Malignant brain tumor with rhabdoid features in an adult. *Neurol Med Chir* **51**, 449–454.

[2] Momota H, Iwami K, Fujii M, Motomura K, and Natsume A, et al (2011). Rhabdoid glioblastoma in a child: case report and literature review. *Brain Tumor Pathol* **28**, 65–70.

[3] Wyatt-Ashmead J, Kleinschmidt-DeMasters BK, Hill DA, Mierau GW, and McGavran L, et al (2001). Rhabdoid glioblastoma. *Clin Neuropathol* **20**, 248–255.

[4] Lath R, Unosson D, Blumbergs P, Stahl J, and Brophy BP (2003). Rhabdoid glioblastoma: a case report. *J Clin Neurosci* **10**, 325–328.

[5] He MX and Wang JJ (2011). Rhabdoid glioblastoma: case report and literature review. *Neuropathology* **31**, 421–426.

[6] Fung KM, Perry A, Payner TD, and Shan Y (2004). Rhabdoid glioblastoma in an adult. *Pathology* **36**, 585–587.

[7] Endo S, Terasaka S, Yamaguchi S, Ikeda H, and Kato T, et al (2013). Primary rhabdoid tumor with low grade glioma component of the central nervous system in a young adult. *Neuropathology* **33**, 185–191.

[8] Kleinschmidt-DeMasters BK, Alassiri AH, Birks DK, Newell KL, Moore W, and Lillehei KO (2010). Epithelioid versus rhabdoid glioblastomas are distinguished by monosomy 22 and immunohistochemical expression of INI-1 but not claudin 6. *Am J Surg Pathol* **34**, 341–354.

[9] Babu R, Hatef J, McLendon RE, Cummings TJ, and Sampson JH, et al (2013). Clinicopathological characteristics and treatment of rhabdoid glioblastoma. *J Neurosurg* **119**, 412–419.

[10] Hiroyuki M, Ogino J, Takahashi A, Hasegawa T, and Wakabayashi T (2015). Rhabdoid glioblastoma: an aggressive variaty of astrocytic tumor. *Nagoya J Med Sci* **77**, 321–328.

[11] Kleinschmidt-DeMasters BK, Aisner DL, Birks DK, and Foreman NK (2013). Epithelioid GBMs show a high percentage of BRAF V600E mutation. *Am J Surg Pathol* **37**, 685–698.

[12] Lee RS, Stewart C, Carter SL, Ambrogio L, and Cibulskis K, et al (2012). A remarkably simple genome underlies highly malignant pediatric rhabdoid cancers. *J Clin Invest* **122**, 2983–2988.

[13] Hasselblatt M, Isken S, Linge A, Eikmeier K, and Jeibmann A, et al (2013). High-resolution genomic analysis suggests the absence of recurrent genomic alterations other than SMARCB1 aberrations in atypical teratoid/rhabdoid tumors. *Genes Chromosomes Cancer* **52**, 185–190.

[14] Louis DN (2007). International Agency for Research on Cancer. WHO classification of tumours of the central nervous system. Lyon: International Agency for Research on Cancer; 2007 [309 p. pp.].

[15] Li H and Durbin R (2009). Fast and accurate short read alignment with Burrows-Wheeler transform. *Bioinformatics* **25**, 1754–1760.

[16] McKenna A, Hanna M, Banks E, Sivachenko A, and Cibulskis K, et al (2010). The Genome Analysis Toolkit: a MapReduce framework for analyzing next-generation DNA sequencing data. *Genome Res* **20**, 1297–1303.

[17] Cingolani P, Platts A, Wang le L, Coon M, and Nguyen T, et al (2012). A program for annotating and predicting the effects of single nucleotide polymorphisms, SnpEff: SNPs in the genome of Drosophila melanogaster strain w1118; iso-2; iso-3. *Fly* **6**, 80–92.

[18] Huillard E, Hashizume R, Phillips JJ, Griveau A, and Ihrie RA, et al (2012). Cooperative interactions of BRAFV600E kinase and CDKN2A locus deficiency in pediatric malignant astrocytoma as a basis for rational therapy. *Proc Natl Acad Sci U S A* **109**, 8710–8715.

[19] McPherson A, Hormozdiari F, Zayed A, Giuliany R, and Ha G, et al (2011). deFuse: an algorithm for gene fusion discovery in tumor RNA-Seq data. *PLoS Comput Biol* **7**, e1001138.

[20] Chen K, Wallis JW, Kandoth C, Kalicki-Veizer JM, and Mungall KL, et al (2012). BreakFusion: targeted assembly-based identification of gene fusions in whole transcriptome paired-end sequencing data. *Bioinformatics* **28**, 1923–1924.

[21] Iyer MK, Chinnaiyan AM, and Maher CA (2011). ChimeraScan: a tool for identifying chimeric transcription in sequencing data. *Bioinformatics* **27**, 2903–2904.

[22] Mortazavi A, Williams BA, McCue K, Schaeffer L, and Wold B (2008). Mapping and quantifying mammalian transcriptomes by RNA-Seq. *Nat Methods* **5**, 621–628.

[23] Shugay M, Ortiz de Mendibil I, Vizmanos JL, and Novo FJ (2013). Oncofuse: a computational framework for the prediction of the oncogenic potential of gene fusions. *Bioinformatics* **29**, 2539–2546.

[24] Van Loo P, Nordgard SH, Lingjaerde OC, Russnes HG, and Rye IH, et al (2010). Allele-specific copy number analysis of tumors. *Proc Natl Acad Sci U S A* **107**, 16910–16915.

[25] Vogelstein B, Papadopoulos N, Velculescu VE, Zhou S, Diaz Jr LA, and Kinzler KW (2013). Cancer genome landscapes. *Science* **339**, 1546–1558.

[26] Sottoriva A, Spiteri I, Piccirillo SG, Touloumis A, and Collins VP, et al (2013). Intratumor heterogeneity in human glioblastoma reflects cancer evolutionary dynamics. *Proc Natl Acad Sci U S A* **110**, 4009–4014.

[27] Kita D, Yonekawa Y, Weller M, and Ohgaki H (2007). PIK3CA alterations in primary (de novo) and secondary glioblastomas. *Acta Neuropathol* **113**, 295–302.

[28] Fuller GN and Scheithauer BW (2007). The 2007 Revised World Health Organization (WHO) Classification of Tumours of the Central Nervous System: newly codified entities. *Brain Pathol* **17**, 304–307.

[29] Byeon SJ, Cho HJ, Baek HW, Park CK, and Choi SH, et al (2014). Rhabdoid glioblastoma is distinguishable from classical glioblastoma by cytogenetics and molecular genetics. *Hum Pathol* **45**, 611–620.

[30] Fassl A, Tagscherer KE, Richter J, Berriel Diaz M, and Alcantara Llaguno SR, et al (2012). Notch1 signaling promotes survival of glioblastoma cells via EGFR-mediated induction of anti-apoptotic Mcl-1. *Oncogene* **31**, 4698–4708.

[31] Natarajan S, Li Y, Miller EE, Shih DJ, and Taylor MD, et al (2013). Notch1-induced brain tumor models the sonic hedgehog subgroup of human medulloblastoma. *Cancer Res* **73**, 5381–5390.

[32] Ehrman LA, Mu X, Waclaw RR, Yoshida Y, and Vorhees CV, et al (2013). The LIM homeobox gene Isl1 is required for the correct development of the striatonigral pathway in the mouse. *Proc Natl Acad Sci U S A* **110**, E4026-4035.

[33] Agaimy A, Erlenbach-Wunsch K, Konukiewitz B, Schmitt AM, and Rieker RJ, et al (2013). ISL1 expression is not restricted to pancreatic well-differentiated neuroendocrine neoplasms, but is also commonly found in well and poorly differentiated neuroendocrine neoplasms of extrapancreatic origin. *Mod Pathol* **26**, 995–1003.

[34] Deng Y, Yao L, Chau L, Ng SS, and Peng Y, et al (2003). N-Myc downstream-regulated gene 2 (NDRG2) inhibits glioblastoma cell proliferation. *Int J Cancer* **106**, 342–347.

[35] Versteege I, Sevenet N, Lange J, Rousseau-Merck MF, and Ambros P, et al (1998). Truncating mutations of hSNF5/INI1 in aggressive paediatric cancer. *Nature* **394**, 203–206.

[36] Roberts CW, Leroux MM, Fleming MD, and Orkin SH (2002). Highly penetrant, rapid tumorigenesis through conditional inversion of the tumor suppressor gene Snf5. *Cancer Cell* **2**, 415–425.

[37] Knutson SK, Warholic NM, Wigle TJ, Klaus CR, and Allain CJ, et al (2013). Durable tumor regression in genetically altered malignant rhabdoid tumors by inhibition of methyltransferase EZH2. *Proc Natl Acad Sci U S A* **110**, 7922–7927.